Angewandte Chemie
Eine Zeitschrift der Gesellschaft Deutscher Chemiker

Supporting Information

69451 Weinheim, Germany

An Aggregation-Induced-Emission Platform for Direct Visualization of Interfacial Dynamic Self-Assembly**

Junwei Li, Yuan Li, Carrie Y. K. Chan, Ryan T. K. Kwok, Hongkun Li, Pavel Zrazhevskiy, Xiaohu Gao, Jing Zhi Sun, Anjun Qin, and Ben Zhong Tang**

anie_201408757_sm_miscellaneous_information.pdf
anie_201408757_sm_movie.avi

TABLE OF CONTENTS

EXPERIMENTAL SECTION

Chemicals and Instrumentation. Tetrahydrofuran (THF) was distilled from sodium benzophenone ketyl under dry nitrogen immediately prior to use. Polystyrene (M_w = 197,000 g mol^{-1}, M_w/M_n = 1.05), solvents, such as chloroform ($CHCl_3$), dichloromethane (DCM), acetone, dimethylsulfoxide (DMSO), and dimethylformamide (DMF), and other reagents were purchased from Aldrich and used as received without further purification.

Field emission scanning electron microscope (FESEM, Sirion-100, FEI) was used for examination of the surface morphology after specimen sputtering with gold using ion sputter JFC-1100. Images were analyzed using ImageJ software (v1.42q, by Wayne Rasband). Fluorescence micrographs were taken on an upright fluorescence microscope Olympus BX41. The images were taken using a computer-controlled SPOTRT SE 18 Mono charge-coupled device (CCD) camera. Video was recorded with a camera under UV lamp illumination in the dark. A hygrothermograph (DT-321S, CEM Corporation) was used to measure the humidity. Milton Ray Spectronic 3000 Array spectrophotometer was used to record the absorption spectra. PerkinElmer LS 55 spectrofluorometer was used to record the photoluminescence (PL) spectra.

Synthesis of AIE-active probes. AIE-active P**I**, P**II** and P**III** were synthesized following established procedure.[1] Briefly, P**I** was polymerized from *4,4'*-[*1,2*-Diphenylethenylenebis(*1,4*-phenylene)dioxybis(*1,4*-butylene)dioxy] Dibenzonitrile under nitrogen atmosphere using standard Schlenk technique in a vacuum line system or an inert atmosphere glove box (Vacuum Atmosphere). The polycyclotrimerization reaction was catalyzed by trifluoromethanesulfonic acid (CF_3SO_3H) in *o*-dichlorobenzene (*o*-DCB): 0.25 mmol *4,4'*-[*1,2*-Diphenylethenylenebis(*1,4*-phenylene)dioxybis(*1,4*-butylene)dioxy] Dibenzonitrile was mixed with 1 mmol CF_3SO_3H in 2 mL *o*-DCB and incubated under continuous stirring for 1 hour at room temperature. Then, the polymerization was terminated by pouring the reaction mixture into 300 mL of methanol/hexane solvent mixture (1:5 v/v) via a cotton filter. The precipitates were filtered by a Gooch crucible, washed with methanol and hexane for three times, and finally dried in vacuum overnight at room temperature. Purification of the polymers was done in an open atmosphere. P**II** was synthesized via McMurry coupling reaction. To a mixture of *4*-Hydroxybenzophenone (14.0 mmol) and potassium carbonate (36.2 mmol) in 50 mL acetone *1,2*-Dibromoethane (4 mL, 46.4

mmol) was added, and the mixture was refluxed under stirring for 24 h. After filtration and solvent evaporation, the crude product was purified by a silica gel column. McMurry coupling of the as-prepared white power yielded *1,2*-bis[*4*-(*2*-bromoethoxy)phenyl]-*1,2*-diphenylethene Dibromide, further quaternization of which by triethylamine produced the desirable product (P**II**). P**III** was prepared from the click polymerization of *4,4′*-isopropylidenediphenyl dipropiolate and *1,2*-bis[*4*-(*6*-azido-hexyloxy)phenyl]-*1,2*-diphenylethene. P**III** represented a linear polymer with M_w = 23,900 g mol^{-1}, M_w/M_n = 1.60 (GPC, polystyrene calibration).

Characterization Data for PI. Pale yellow solid. M_w = 16,640 g mol^{-1}; M_w/M_n = 2.23 (GPC, polystyrene calibration); degree of branching about 63%. IR (KBr), υ (cm^{-1}): 3051, 2944, 2872, 2224, 1584, 1507, 1472, 1419, 1369, 1301, 1243, 1172, 1146, 1111, 1015. ^{1}H NMR (300 MHz, DMSO-d_6), δ (ppm): 8.70, 8.68, 7.57, 7.54, 7.08, 7.04, 7.01, 6.95, 6.92, 6.89, 6.66, 6.63, 6.60, 4.13, 4.04, 4.02, 3.98, 3.96, 3.94, 1.98, 1.94. ^{13}C NMR (75 MHz, DMSO-d_6), δ (ppm): 171.4, 163.2, 162.9, 158.2, 158.0, 145.0, 144.9, 140.7, 140.1, 139.9, 137.1, 137.0, 135.0, 134.6, 134.0, 133.3, 132.0, 131.4, 129.7, 128.3, 126.8, 126.7, 119.9, 118.1, 115.8, 115.0, 114.2, 114.2, 106.0, 104.5, 68.6, 68.4, 67.9, 67.7, 26.7, 26.5, 26.5.

Preparation of Nanoaggregates. Stock THF solutions of P**I** with concentrations ranging from 1 mg mL^{-1} to 20 mg mL^{-1} were prepared to yield an identical final P**I** concentration of 1 mg mL^{-1} in THF/water mixtures with composition ranging from 100% THF/0% water to 5% THF/95% water. Nanoaggregates were prepared by adding water to P**I**/THF solution dropwise under vigorous stirring, obtaining a desirable THF-to-water proportion. The PL measurements of the resulting solutions were performed immediately after P**I** nanoaggregate preparation.

Monitoring the evolution of microemulsion. P**I** (50 mg) was dissolved in 5 mL $CHCl_3$ by vortexing for 5 min. Complete polymer dissolution was confirmed by the lack of solution fluorescence measured with spectrofluorometery (excitation wavelength: 310 nm; emission wavelength: 470 nm). Then, 1 mL of as-prepared non-emissive solution was added dropwise into the aqueous solution (9 mL) under sonication at room temperature. A 200 μL emulsion droplet was immediately casted onto a glass slide for examination with fluorescence microscopy at room temperature and about 30% humidity. To capture the fast dynamics of microemulsion evolution,

the microscope objective was pre-focused on the glass slide surface before emulsion casting.

Monitoring the evolution of coffee-ring. P**I** or P**II** (1 mg) were dissolved in $CHCl_3$ (1 mL) or water (1 mL), respectively, by vortexing for 5 min to obtain homogeneous non-fluorescent polymer solutions. Complete polymer dissolution was confirmed by the lack of AIE signal at 470 nm (310 nm excitation) for P**I** and at 450 nm (350 nm excitation) for P**II** using spectrofluorometry. Then, 20 μL of as-prepared solution was casted onto a glass slide for examination of coffee-ring formation with fluorescence microscopy at room temperature and about 30% humidity. To capture the fast dynamics of droplet evaporation and coffee-ring formation, the microscope objective was pre-focused on the glass slide surface before droplet casting.

Monitoring the evolution of breath figures. P**I** (5 mg) was dissolved in 5 mL $CHCl_3$ by vortexing for 5 min to ensure complete polymer dissolution. A glass slide was positioned onto the stage of a fluorescence microscope, and the objective was pre-focused on the glass slide surface. Then, 500 μL of as-prepared non-emissive P**I** solution was quickly casted onto a glass slide to get a uniform liquid film. An air-washing bottle was used to generate a constant 4 L min^{-1} humid airflow above P**I** film by bubbling through the distilled water, increasing humidity around the slide to above 70%, as measured by the hygrothermograph. Preparation of breath figures using P**III** probe and P**I**-doped polystyrene was done in an analogous manner. The bright-field and fluorescence microscopy were used to monitor evolution of breath figures at room temperature. Macroscopic monitoring of breath figure formation and AIE signal evolution was done using a video camera and a handheld UV-lamp excitation.

Computer simulation of breath figures. The Monte Carlo method was used to simulate the dynamic behaviors of the breath figures. Air, Water, $CHCl_3$, and AIE probes were considered as the components of cells, which walk across the whole map through four behaviors: evaporation, surface/interface tension, gravity, and thermal motion. Time dependence was simulated via step-by-step iteration. More details can be found in Figures S10-S12.

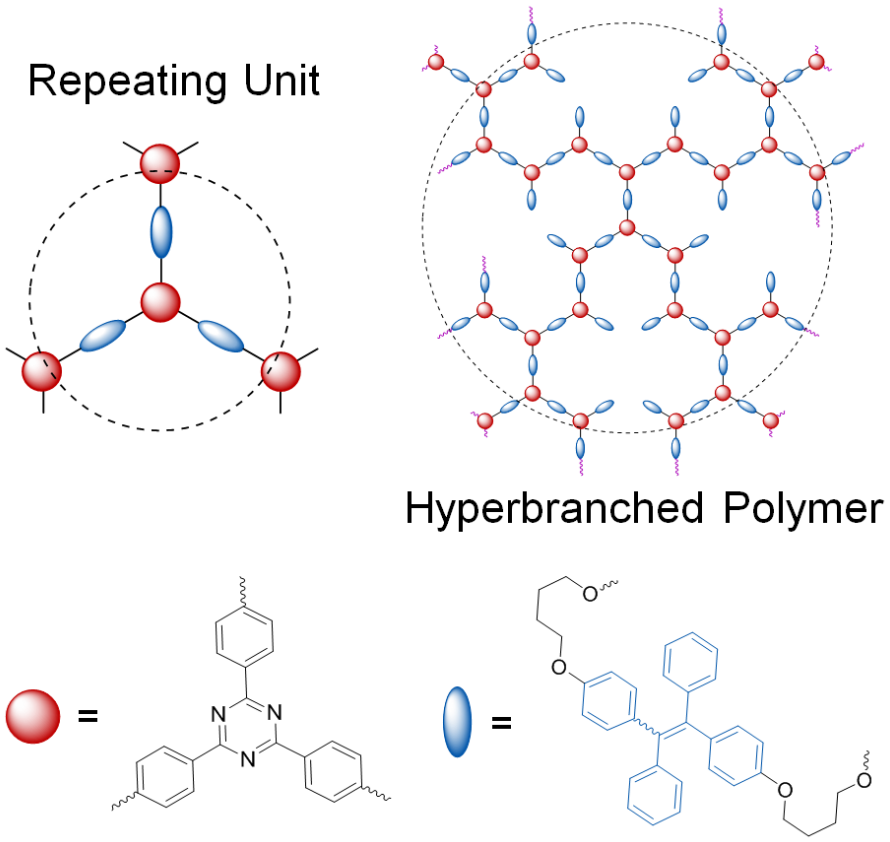

Figure S1. Schematic of the chemical structure of AIE-active probe I (P**I**) and the polymer geometry. AIE-active TPE units (blue) are incorporated into the repeating units of polytriazine (red), generating hyperbranched polymer with aggregation-induced emission properties.

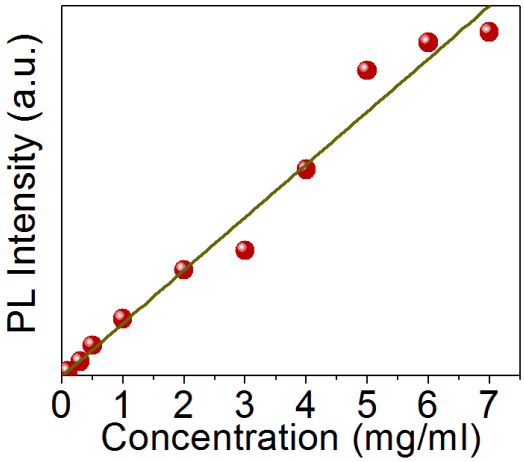

Figure S2. Relationship between the fluorescence intensity and concentration P**I** nanoaggregates in THF/water mixtures with 95% water.

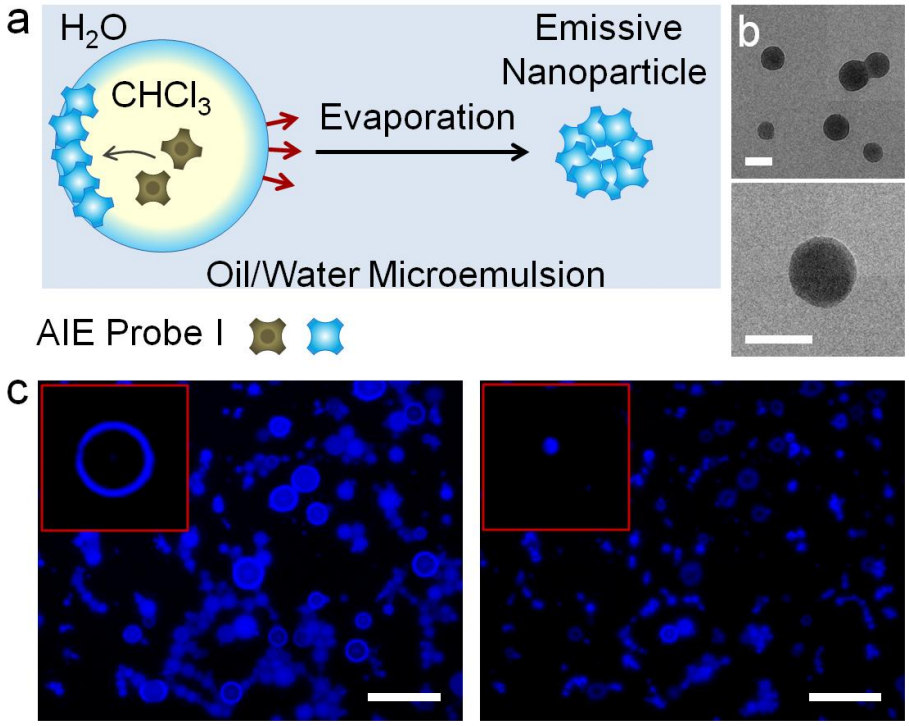

Figure S3. (a) Schematic of oil-in-water microemulsion monitoring via AIE imaging technology. The non-fluorescent AIE probe P**I** dissolved in the "oil" phase (chloroform) turns into high-emissive state only upon phase-inversion at the water/oil boundary due to poor solubility in water. With chloroform evaporation droplets shrink, finally producing nano-sized particles solely composed of highly fluorescent P**I**. (b) Representative TEM images of P**I** nanoparticles prepared via microemulsion. Scale bar, 200 nm. (c) Real-time monitoring of the microemulsion evolution with fluorescence microscopy. A clear highly emissive layer can be observed at the oil-water interface immediately following microemulsion preparation (left panel). In comparison to fluorophores lacking AIE activity, the contrast is dramatically enhanced due to high solubility of P**I** in chloroform, yielding lack of fluorescence from the bulk of "oil" droplets. After 2 minutes, the size of droplets decreases from around 5 μm to 200 nm (right panel), eventually forming highly emissive nanoparticles. Scale bar, 10 μm.

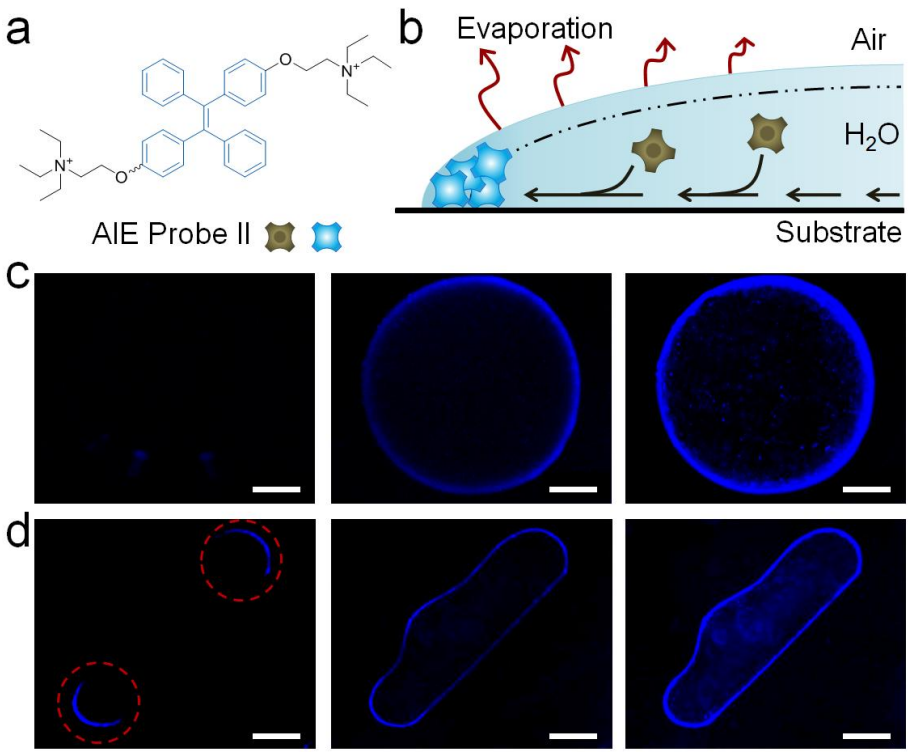

Figure S4. a) Chemical structure of a water-soluble TPE-based AIE-active probe II (P**II**) used for visualizing the coffee-ring formation. b) Schematic of "coffee-ring" formation study using AIE imaging technology. During evaporation and drying process, the droplet-glass contact line remains pinned as fluid carrying AIE probes flows outward from the droplet center to replenish the edges. The probes maintains non-emissive state while fully dissolved inside the droplet; however, when driven by the capillary flow to the air-water interface at the contact line, probes precipitate and experience RIR, turning into a high-fluorescence state and highlighting the stain deposition process. Fluorescence microscopy of circular (c) and rod-shaped (d) P**II** solution droplets reveals initial lack and subsequent increase of P**II** fluorescence upon drying and coffee-ring formation. Interestingly, real-time AIE-based imaging highlights faster precipitation of the probes at the contact line with smaller radius of curvature (d, red circles), consistent with predicted capillary flow patterns induced by small temperatures gradients developing inside droplets upon evaporation. Images were acquired at 5, 10 and 15 min (left-to-right) after droplet casting onto a glass slide. Scale bar, 500 μm.

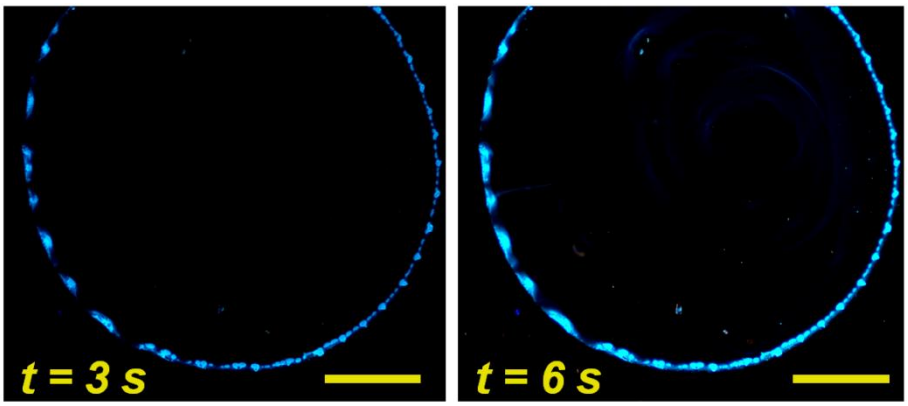

Figure S5. Fluorescence microscopy images of coffee-ring structure by P**I** in chloroform at 3 s and 6 s. A clear coffee-ring pattern (highly emissive circle around the edge of the droplet) rapidly develops upon chloroform evaporation. Similar to aqueous systems, fully dissolved non-emissive hydrophobic polymer is carried to the air/solvent interface by the capillary flow, resulting in P**I** precipitation and activation of AIE fluorescence. Thus, AIE-based imaging can be successfully employed for real-time observation of dynamic processes at liquid/air interfaces in both aqueous and organic solvent systems. Scale bars, 500 μm.

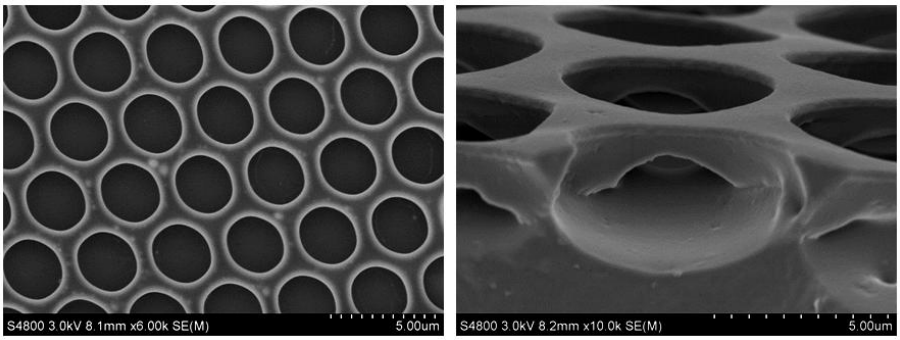

Figure S6. SEM images of the ordered porous films formed by P**I** via breath figure process. Top view (left) and cross-section (right) are shown.

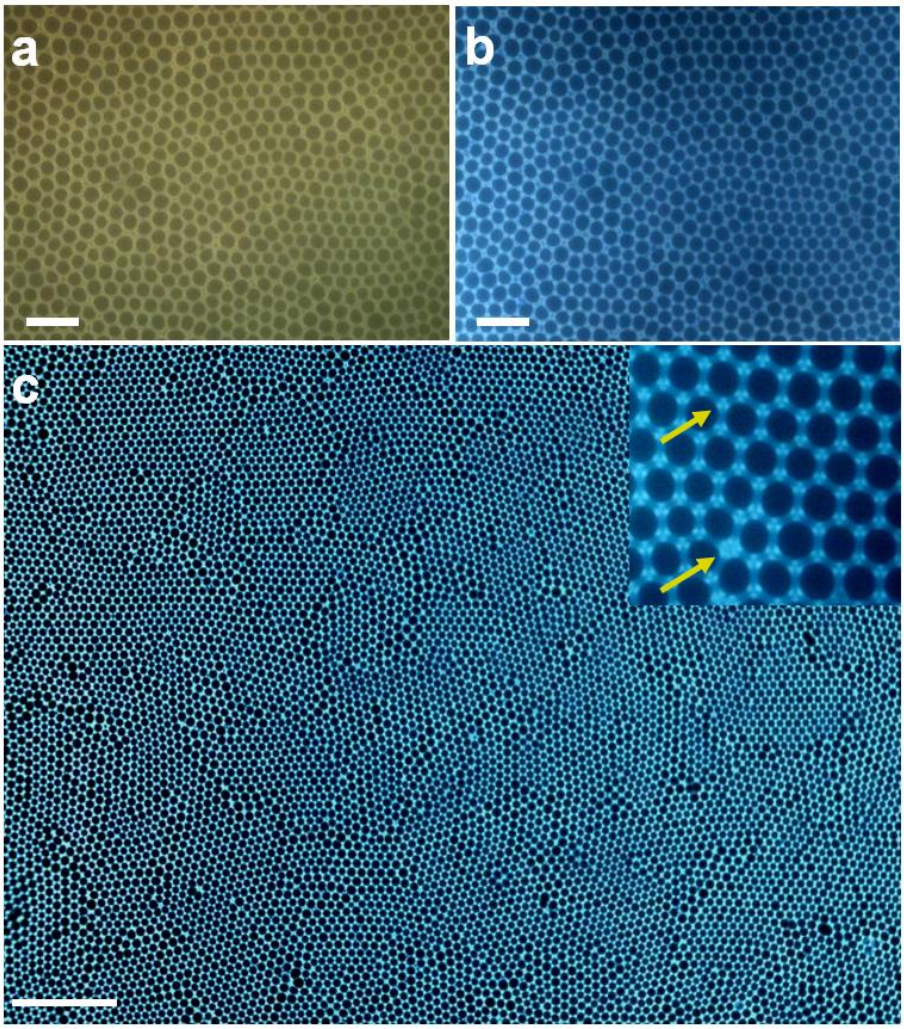

Figure S7. (a) Bright-field and (b) fluorescence microscopy images of breath figures generated with P**I**. Scale bar, 10 μm. Nearly total film transparency and unique AIE properties of P**I** polymer enable high-contrast imaging of breath figure structures with fluorescence microscopy. (c) Wide-field image of the ordered honeycomb-like breath figure pattern. Scale bar, 30 μm. Inset: enlarged image of the clover-like fluorescent structures forming at the pore junctions. Successful formation of characteristic patterns confirms that AIE-active polymer P**I** can serve as both a fluorophore and a structural material for breath figure formation, making it a suitable probe for real-time monitoring of this dynamic process.

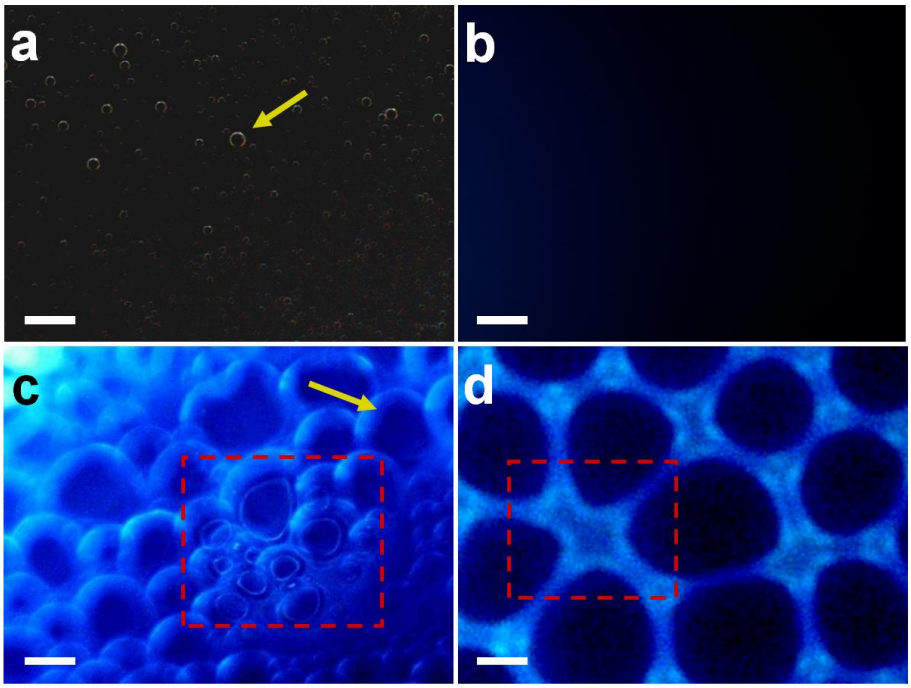

Figure S8. (a) Bright-field and (b) fluorescence microscopy images of the water nucleation stage (Step 1) of breath figure formation. Scale bar, 5 μm. Yellow arrow shows one water droplet under low-illumination bright-field imaging modality, which is invisible under fluorescence modality. Both images were taken back-to-back from the same area of view. (c) The dynamic process of gap bursting in random directions (Step 3) captured by fluorescence microscopy. Scale bar, 2 μm. Yellow arrow shows one bursting gap that forms at the back of the droplet. Enhancement of fluorescence around gap edges indicates likely P**I** probe enrichment at the boundaries with smaller radius of curvature due to capillary flow (analogously to coffee-ring formation mechanism, Figure S4, S5). Furthermore, visualization of the bursting layers on top of droplets provides additional evidence in support of a thin polymer film deposition on water droplets during Step 2. (d) Polymer enrichment at the pore boundaries highlighted by AIE-based fluorescence microscopy. Scale bar, 1 μm. Typically, a "clover-like" fluorescent pattern could be formed at the junction of three nearby droplets. Assembly of four or more water droplets together during breath figure formation, instead, yielded high fluorescence enrichment around the pores.

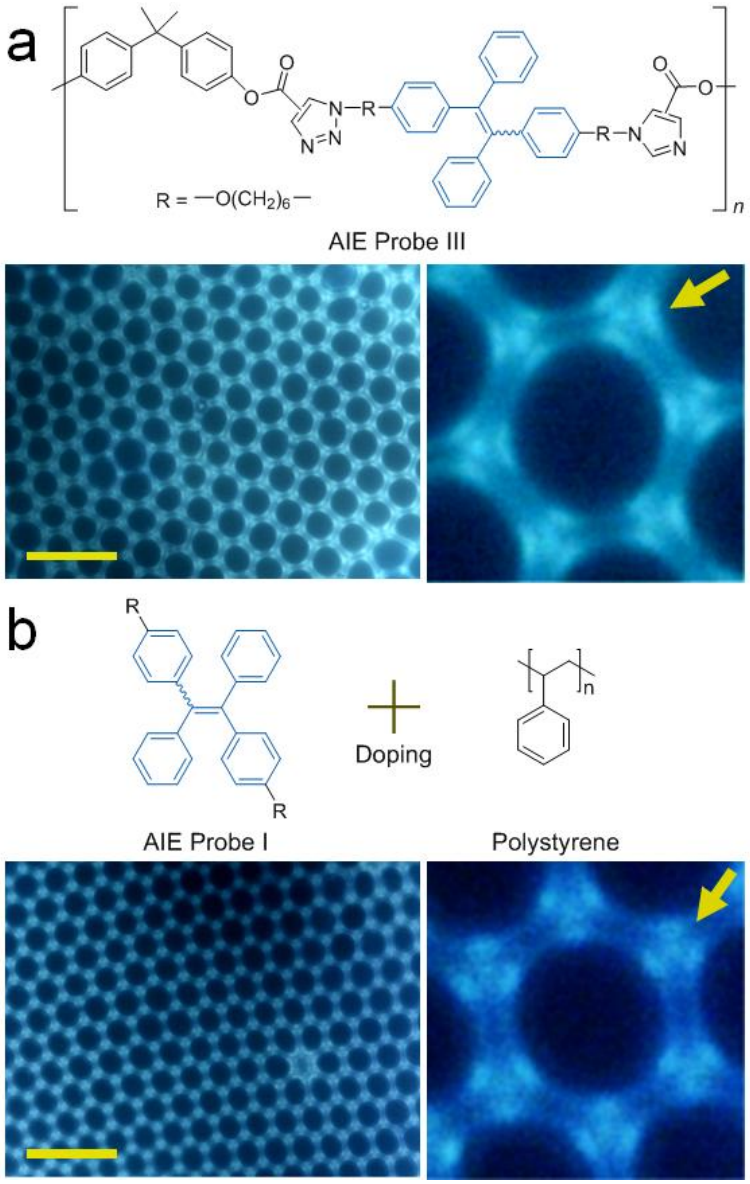

Figure S9. (a) Chemical structure of a linear hydrophobic polymeric TPE-based AIE-active probe (P**III**, M_w = 23,900 g mol^{-1}; M_w/M_n = 1.60) and fluorescence microscopy images of breath figures generated with P**III** (1 mg mL^{-1} in $CHCl_3$). Scale bar, 10 μm. (b) Fluorescence microscopy images of breath figures generated with P**I**-doped polystyrene (M_w = 197,000 g mol^{-1}; M_w/M_n = 1.05; 1 mg mL^{-1} in $CHCl_3$; 1:1 w/w P**I**-to-polystyrene ratio). Scale bar, 10 μm. Similar to breath figures made with hyperbranched P**I** polymer, characteristic ordered films with clover-like fluorescent patterns (yellow arrow) could be produced by a linear P**III** polymer (a) as well as P**I**-doped polystyrene (b), demonstrating compatibility of the AIE imaging platform with alternative material compositions.

THEORETICAL ANALYSIS

Differential pressure, ΔP, induced by the surface tension of the top layer across the meniscus is defined by Equation (S1):[2]

$$\Delta P = \frac{2\gamma_1 + 2\gamma_2}{R} \quad \text{(S1)}$$

where γ_1 is the surface tension of the thin film, γ_2 is the interface tension of the water/thin film interface, and R is the radius of the meniscus. For calculation of ΔP developed by P**I** polymer it was assumed that the values of γ_1, γ_2 were equal and R coincided with the radius of encapsulated droplets. Literature values of $\gamma_1 = \gamma_2 = 25.6$ mN m^{-1} for polystyrene were used.[3]

Critical differential pressure, ΔP_c, of the polymer film is defined by Equation (S2):[4]

$$\Delta P_c = \frac{4E}{3}\left(\frac{\delta}{R}\right)^2 \quad \text{(S2)}$$

where δ is the thickness of the thin film, E is Young's modulus of the polymer. An estimated film thickness of about 15 nm and literature value of E = 150 MPa for polystyrene were used for ΔP_c calculation.[5]

The bursting pressure was defined as the difference between ΔP and ΔP_c. Positive bursting pressure developed for R > 439 nm, reaching its maximum value of 58.3 KPa at R = 878 nm. When R increased to 10 μm, the bursting pressure decreased to 9.91 KPa, which was only 17% of the highest value. Further increase of R to 2 mm yielded the bursting pressure of a mere 0.88% of the highest value.

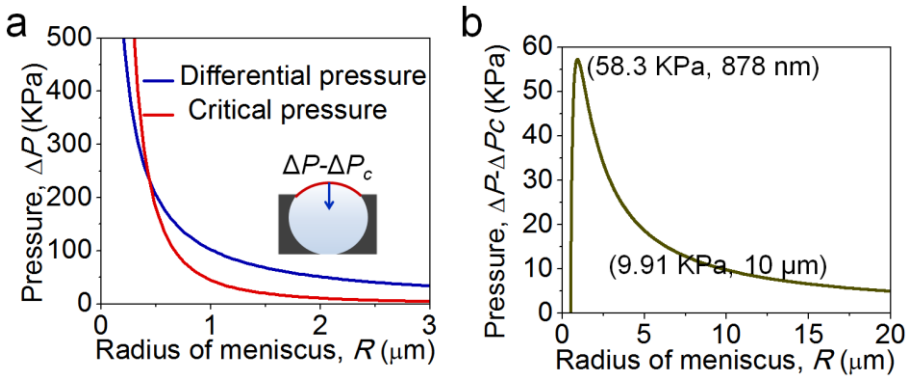

Figure S10. Theoretical analysis of bursting gap formation within the P**I**/chloroform film encapsulating water droplets. a) Calculated curves of differential pressure (ΔP) and critical differential pressure (ΔP_c) vs. the droplet radius. Inset: schematic of the bursting gap formation. (b) Calculated curve of bursting pressure (ΔP-ΔP_c) vs. the radius. The bursting pressure reached the highest value of 58.3 KPa for R = 878 nm, while dramatically decreasing to only 9.91 KPa (17% of maximum) when *R* increased to 10 μm.

SIMULATION METHOD

The Monte Carlo method is used to simulate the dynamic behaviors of gap bursting in the formation of breath figures. Water, chloroform and AIE probes are considered as the components of each cell, as shown in Figure S10. These cells walk across the map through four behaviors: evaporation, tension, gravity, and thermal motion. The behaviors of different species in this simulation are listed in Table S1. Air is assumed to be a passive species that only fills the gap in the constitution map.

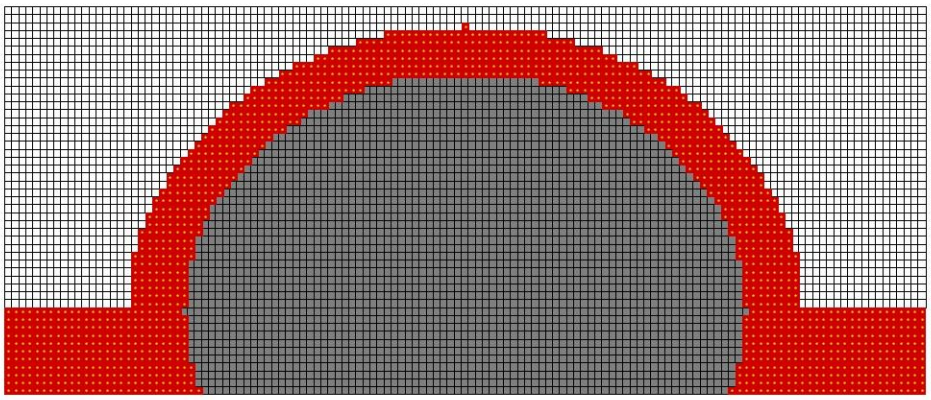

Figure S11. Cellularing the species as a constitution map. White, red, and gray cells represent air, chloroform and water, respectively. The PI distributed in chloroform homogeneously is shown in yellow.

Table S1. Behaviors of different species in the simulation of breath figure formation.

species	evaporation	tension	gravity	thermal motion
water	Y	Y	Y	N
chloroform	Y	Y	Y	Y
AIE probe	N	Y	Y	Y
air	N	N	N	N

Y = yes, N = no.

In the simulation, the probability of evaporation of one cell (water or chloroform) is related to the surrounding air cells via Equation (S3):

$$P_{evaporation} = Exp\left[\frac{Log[2]}{N_{\max}^{a}}(x)^{a}\right] - 1 \qquad \text{(S3)}$$

where, N_{max} = 100, is the maximum cell number surrounding one cell at a certain distance range, and the constant α is related to the material properties (i.e. properties of chloroform and water).

The force of tension onto a cell is defined as the resultant force from surrounding cells in the range of r_t = 4 (Figure S11).

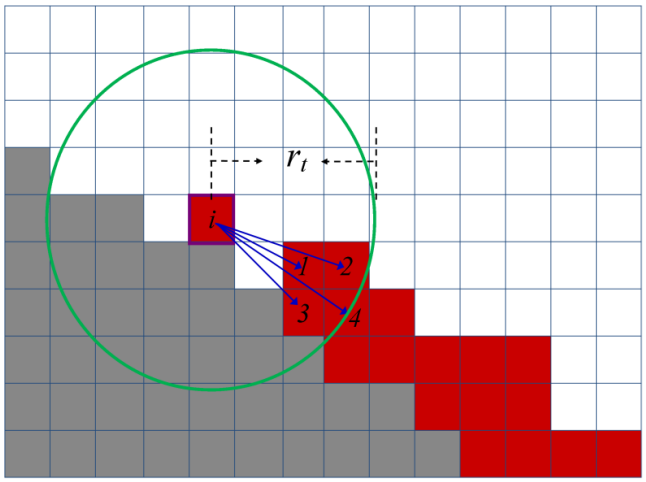

Figure S12. Tension effect on cell i. The cell i is pulled by the surrounding cells 1-4 in the range of r_t.

After cell evaporation, the temperature of cells surrounding the one evaporated goes down by ΔT as defined by Equation (S4), creating temperature gradient on the surface (Figure S12).

$$T_{i+1} = T_i - \Delta T \tag{S4}$$

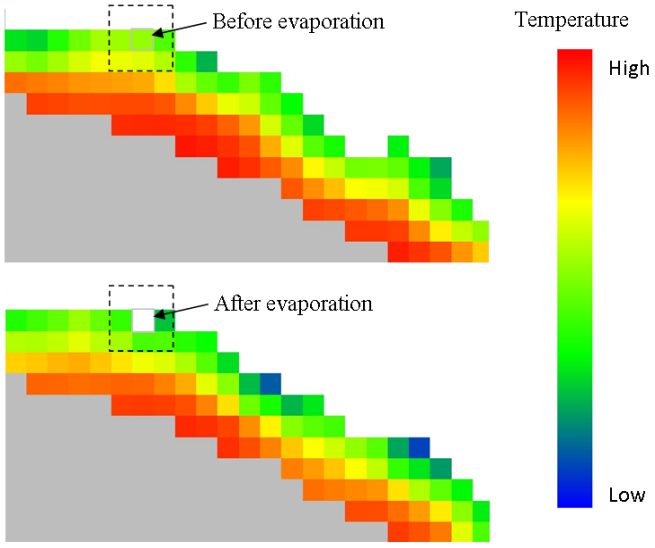

Figure S13. Temperature distributions in chloroform before and after evaporation of one cell. The dashed area shows that the temperature in surrounding area drops (color: blue shift) after the center cell evaporated.

Temperature gradient induces the capillary flow, which carries AIE-active probes in the solution towards the position with a lower temperature potential.

SIMULATION ALGORITHM

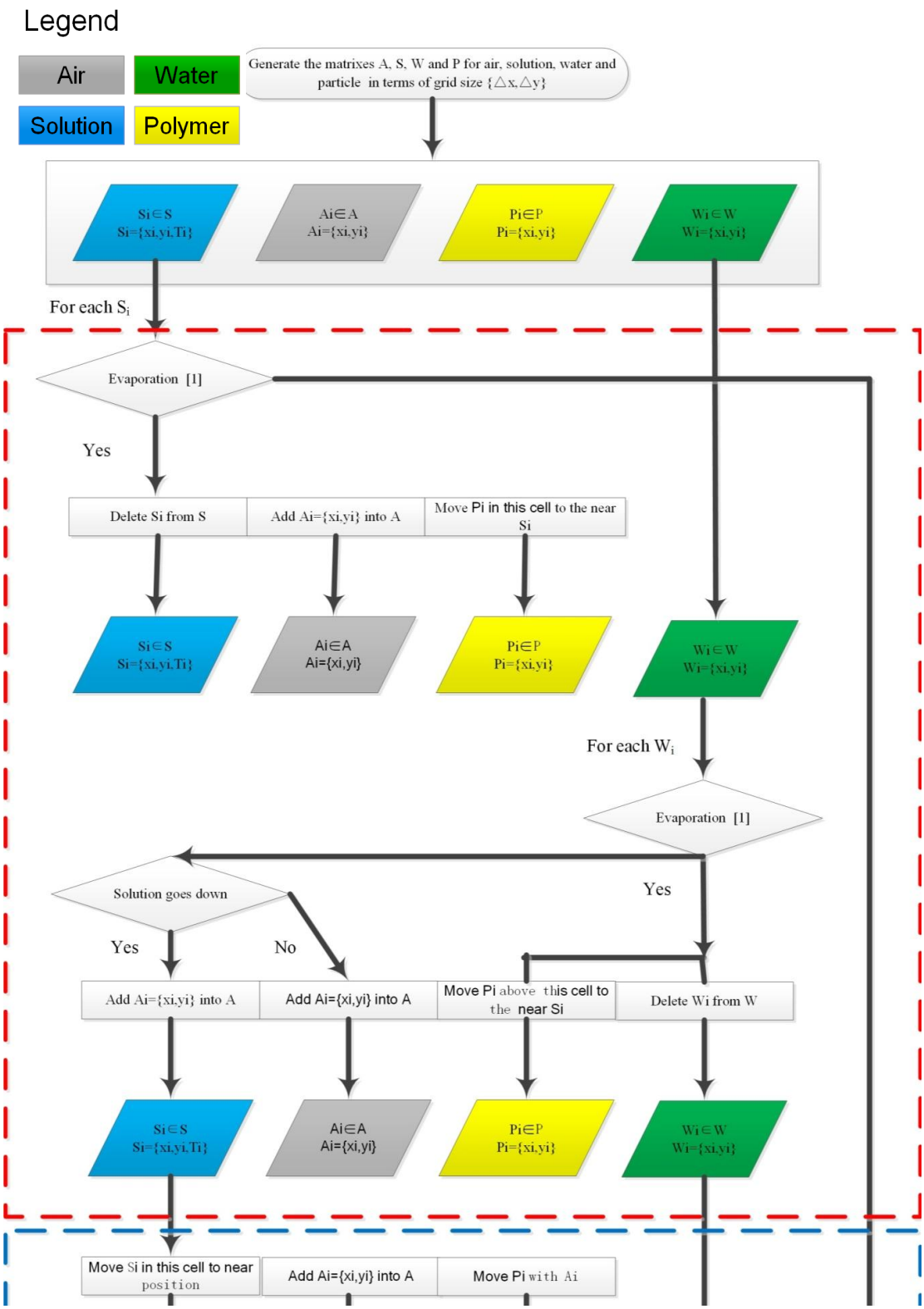

Continued on p.S19

Continued from p.S18

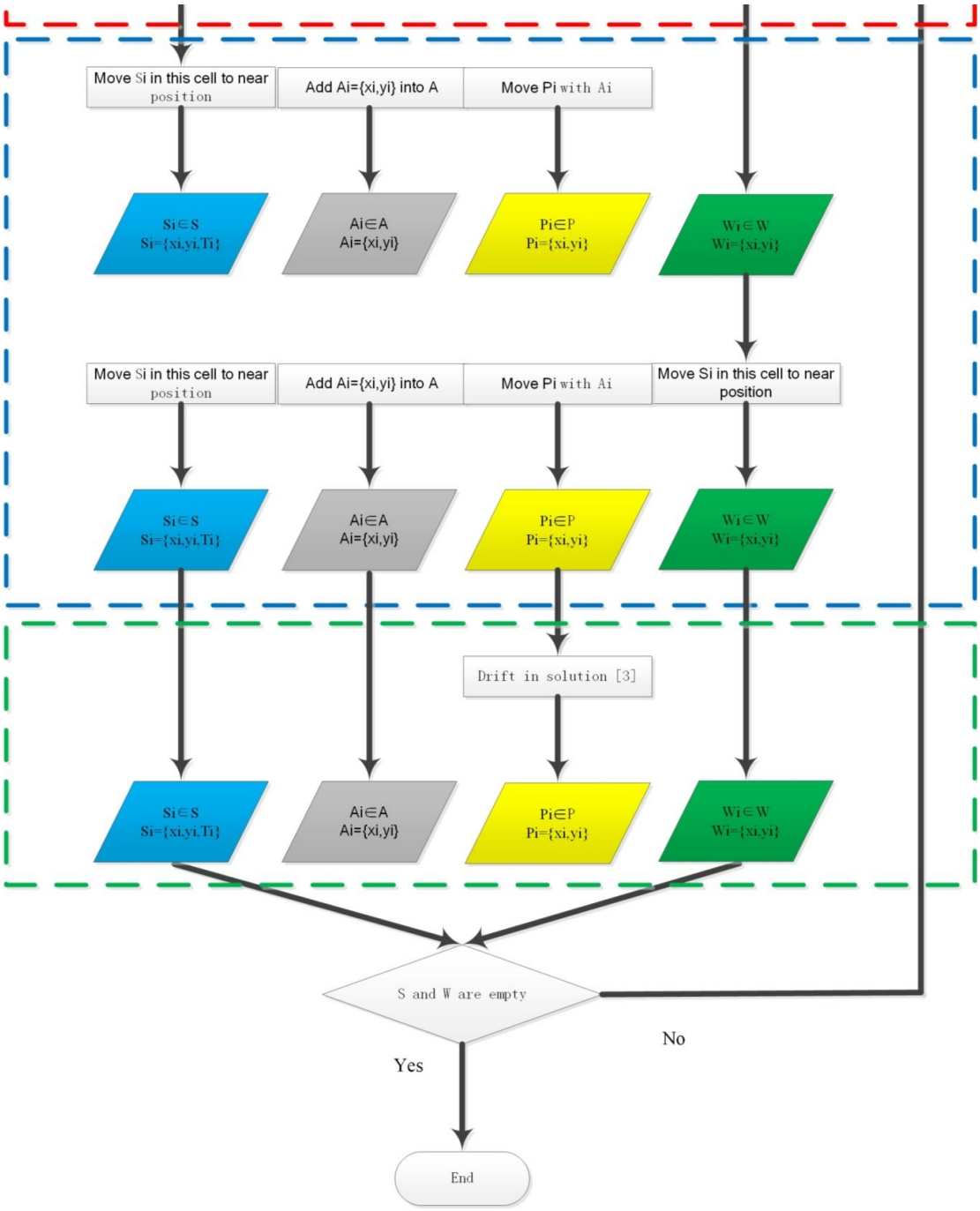

REFERENCES

[1] a) C. Y. Chan, J. W. Lam, C. K. Jim, H. H. Sung, I. D. Williams, B. Z. Tang, *Macromolecules* **2013**, *46*, 9494-9506; b) Y. Hong, H. Xiong, J. W. Y. Lam, M. Häussler, J. Liu, Y. Yu, Y. Zhong, H. H. Sung, I. D. Williams, K. S. Wong, *Chem. Eur. J.* **2010**, *16*, 1232-1245.

[2] J. P. Youngblood, T. J. McCarthy, *Macromolecules* **1999**, *32*, 6800-6806.

[3] D. R. Absolom, A. W. Neumann, *Colloids Surf.* **1987**, *30*, 25-45.

[4] a) C. Gao, S. Leporatti, S. Moya, E. Donath, H. Möhwald, *Langmuir* **2001**, *17*, 3491-3495; b) L.-S. Wan, J.-W. Li, B.-B. Ke, Z.-K. Xu, *J. Am. Chem. Soc.* **2012**, *134*, 95-98.

[5] a) G. R. Guillen, Y. Pan, M. Li, E. M. Hoek, *Ind. Eng. Chem. Res.* **2011**, *50*, 3798-3817; b) J. M. Torres, C. M. Stafford, B. D. Vogt, *Polymer* **2010**, *51*, 4211-4217.